Integrated interferometric approach to solve microring resonance splitting in biosensor applications

Sam Werquin,[1,2,*] Steven Verstuyft,[1] and Peter Bienstman[1,2]

[1] *Photonics Research Group, INTEC Department, Ghent University - imec, Sint-Pietersnieuwstraat 41, 9000 Gent, Belgium*
[2] *Center for Nano- and Biophotonics (NB-Photonics), Ghent University, Belgium*
[*] *sam.werquin@intec.ugent.be*

Abstract: Silicon-on-insulator microring resonators have proven to be an excellent platform for label-free nanophotonic biosensors. The high index contrast of silicon-on-insulator allows for fabrication of micrometer-size sensors. However, it also limits the quality of the resonances by introducing an intrinsic mode-splitting. Backscattering of optical power at small waveguide variations lifts the degeneracy of the normal resonator modes. This severely deteriorates the quality of the output signal, which is of utmost importance to determine the performance of the microrings as a biosensor. We suggest an integrated interferometric approach to give access to the unsplit, high-quality normal modes of the microring resonator and experimentally show an improvement of the quality factor by a factor of 3.

OCIS codes: (130.3120) Integrated optics devices; (130.6010) Sensors; (230.5750) Resonators.

References and links

1. K. De Vos, J. Girones, T. Claes, Y. De Koninck, S. Popelka, E. Schacht, R. Baets, and P. Bienstman, "Multiplexed antibody detection with an array of silicon-on-insulator microring resonators," IEEE Photon. J. **1**, 225–235 (2009).
2. M. Iqbal, M. A. Gleeson, B. Spaugh, F. Tybor, W. G. Gunn, M. Hochberg, T. Baehr-Jones, R. C. Bailey, and L. C. Gunn, "Label-free biosensor arrays based on silicon ring resonators and high-speed optical scanning instrumentation," IEEE J. Sel. Topics Quantum Electron. **16**, 654–661 (2010).
3. C. L. Arce, K. D. Vos, T. Claes, K. Komorowska, D. V. Thourhout, and P. Bienstman, "Silicon-on-insulator microring resonator sensor integrated on an optical fiber facet," IEEE Photon. Technol. Lett. **23**, 890–892 (2011).
4. T. Claes, W. Bogaerts, and P. Bienstman, "Experimental characterization of a silicon photonic biosensor consisting of two cascaded ring resonators based on the Vernier-effect and introduction of a curve fitting method for an improved detection limit," Opt. Express **18**, 22747–22761 (2010).
5. J. Wang and D. Dai, "Highly sensitive Si nanowire-based optical sensor using a Mach Zehnder interferometer coupled microring," Opt. Lett. **35**, 4229–4231 (2010).
6. W. Bogaerts, P. D. Heyn, T. V. Vaerenbergh, K. D. Vos, S. Kumar, T. Claes, P. Dumon, P. Bienstman, D. V. Thourhout, and R. Baets, "Silicon microring resonators," Laser Photonics Rev. **6**, 47–73 (2011).
7. T. Claes, J. Molera, K. De Vos, E. Schacht, R. Baets, and P. Bienstman, "Label-free biosensing with a slot-waveguide-based ring resonator in silicon on insulator," IEEE Photon. J. **1**, 197–204 (2009).
8. T. J. Kippenberg, S. M. Spillane, and K. J. Vahala, "Modal coupling in traveling-wave resonators." Opt. Lett. **27**, 1669–71 (2002).
9. B. E. Little, J. P. Laine, and S. T. Chu, "Surface-roughness-induced contradirectional coupling in ring and disk resonators." Opt. Lett. **22**, 4–6 (1997).
10. B. Little, S. Chu, H. Haus, J. Foresi, and J.-P. Laine, "Microring resonator channel dropping filters," J. Lightw. Technol. **15**, 998–1005 (1997).

11. J. Knittel, T. G. McRae, K. H. Lee, and W. P. Bowen, "Interferometric detection of mode splitting for whispering gallery mode biosensors," Appl. Phys. Lett. **97**, 123704 (2010).
12. J. Hu, X. Sun, A. Agarwal, and L. C. Kimerling, "Design guidelines for optical resonator biochemical sensors," J. Opt. Soc. Am. B **26**, 1032–1041 (2009).
13. G. Roelkens, D. Vermeulen, R. Selvaraja, SHalir, W. Bogaerts, and D. V. Thourhout, "Grating-based optical fiber interfaces for silicon-on-insulator photonic integrated circuits," IEEE J. Sel. Topics Quantum Electron. **17**, 571–580 (2011).
14. The Dow Chemical Company, "Cyclotene advanced electronics resins," (2013), http://www.dow.com/cyclotene/prod/402235.htm.
15. S. Stankovic, R. Jones, J. Heck, M. Sysak, D. Van Thourhout, and G. Roelkens, "Die-to-die adhesive bonding procedure for evanescently-coupled photonic devices," Electrochem. Solid-State Lett. **14**, H326 (2011).
16. K. V. Acoleyen, K. Komorowska, and W. Bogaerts, "One-dimensional off-chip beam steering and shaping using optical phased arrays on silicon-on-insulator," J. Lightw. Technol. **29**, 3500–3505 (2011).

1. Introduction

Silicon-on-insulator (SOI) microring resonators have proven to be an excellent platform for label-free nanophotonic biosensors. The high index contrast of SOI allows for fabrication of micrometer-size sensors, which makes microring resonators excellent candidates for highly multiplexed assays [1, 2]. It also allows for integration of a sensor on an optical fiber tip, opening the door to in-vivo applications [3]. By combining microrings in advanced sensing configurations, it is also shown that their sensitivity can be improved significantly [4, 5]. The high index contrast of the SOI-platform causes high confinement of the optical fields in the waveguides, which makes the microrings very sensitive to changes on the waveguide surface. This explains their very high sensitivity to biomaterials, but at the same time, waveguide roughness causes scattering of the guided light. This degrades the quality factor of the resonances and can ultimately lead to splitting of the resonance [6]. Because the detection limit of a microring biosensor is directly related to the quality of the ring resonance, a high Q-factor is of primordial importance in sensing applications [7]. When implementing the microring sensor as a biosensor, concequences of resonance splitting can become even worse. In a biosensor device, the resonance wavelength will be tracked automatically by a fitting algorithm. This works fine for unsplit resonances, but unpredictable resonance splitting can introduce aliasing in the recorded binding curve signal. Since the resonance splitting in a microring sensor can easily amount to a measurable erroneous shift, unexpected resonance splitting can result in fitting errors and severely compromise a recorded binding curve. As it is partly a consequence of random process variations on the waveguide edges, it is impossible to predict its strength. Therefore, the influence of resonance splitting can be more severe than limiting the detection limit. Jumps between both modes of a split resonance can lead to false positive or even false negative results when the sensor is implemented in a lab-on-a-chip setting. In this paper, we present an integrated interferometric approach to resolve the resonance splitting of a microring resonantor on a single chip. A theoretical model is confirmed by experimental results and an improvement of the resonance quality by a factor of 3 is obtained.

2. Origin of resonance splitting

A perfectly symmetric microring resonator mode in the absense of a bus waveguide is twofold degenerate. Both clockwise (CW) and counterclockwise (CCW) propagation are possible in the microring and both modes are uncoupled. This degeneracy is lifted when the CW-mode and CCW-mode become coupled, e.g. by surface roughness on the waveguide edges and by the proximity of bus waveguides. These deviations from circular symmetry cause forward propagating light to scatter back into the opposite direction, exciting a CCW-mode from a CW-mode and vice versa. Standing-wave modes as a symmetric and antisymmetric superposition of the

traveling waves can now be considered as the new eigenmodes of the system. They will however no longer be degenerate as a consequence of the symmetry breaking coupling [8]. If the linewidth of the resonance is small enough to distinguish both modes, the resonance splitting will be visible in the output signal. This occurs for high quality resonances, when the backreflected power exceeds the coupling losses of the resonator. A critical relation between reflected power and microring coupling is derived in [9].

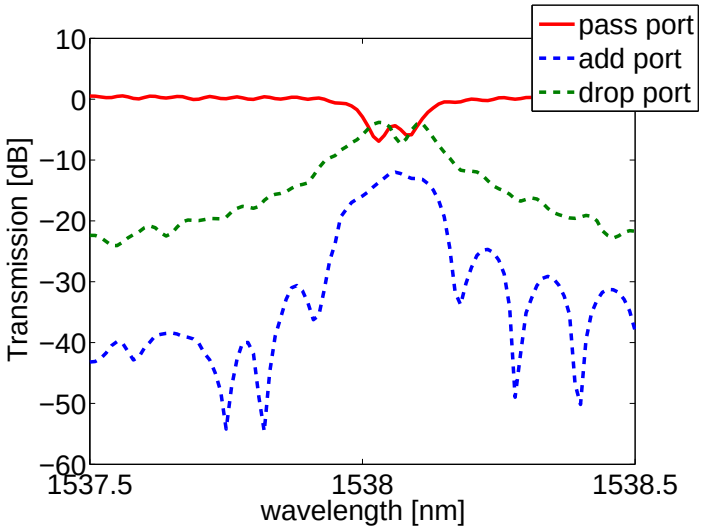

Fig. 1. Measured spectra for add-drop microring resonator showing resonance splitting and backscattered power

Evidence of the importance of backreflected power is provided in figure 1, which shows both the pass-port and add-port spectrum of a microring in add-drop configuration. The microring is designed to have a roundtrip length of $36\mu m$ and a power coupling ratio of 6 percent. Since only the input port is excited, no power should be present in the CCW-mode and the add port should remain dark. The measurement shows that backscattering in the microring waveguide cannot be neglected, resulting in significant power in the add port and resonance splitting in the pass-signal amounting up to 50 pm. Using the simple coupled harmonic oscillator model described in [8], one can easily derive expressions for the CW and CCW-modes of a microring resonator coupled to a waveguide in the all-pass configuration. The coupled mode system is described by by equation 1:

$$\begin{aligned} \frac{da_{CW}}{dt} &= i\Delta\omega a_{CW} - \frac{1}{2\tau}a_{CW} + \frac{i}{2\gamma}a_{CCW} + \kappa s \\ \frac{da_{CCW}}{dt} &= i\Delta\omega a_{CCW} - \frac{1}{2\tau}a_{CCW} + \frac{i}{2\gamma}a_{CW} \end{aligned} \tag{1}$$

Here, a is the amplitude of the CW and CCW-modes ($|a|^2$ is the energy stored in the CW and CCW-modes, respectively) and s represents the field in the input waveguide($|s|^2$ is the input power). The frequency of the lightwave is detuned by $\Delta\omega$ with respect to the resonance frequency of the resonator. τ is the lifetime of photons in the resonator and is determined by the total losses of the coupled microring resonator. The photon lifetime is related to the quality factor (Q) of the microring as $Q = \omega\tau$. κ describes the coupling from the input wave to the resonator mode. By associating a lifetime $\kappa = \sqrt{1/\tau_{ext}}$ to the coupling coefficient, intrinsic resonator losses can be distinguished from coupling losses as $1/\tau = 1/\tau_{ext} + 1/\tau_0$. τ_0 is determined by material absorption and scattering losses in the microring waveguide. Losses in the bends and directional coupler also contribute to the intrinsic amplitude decay in the reso-

nator. As explained in [10], the traditionally used power coupling coefficient K can be readily translated to the coupling coefficient κ used in this description. The coupling between CW and CCW-mode is described by the scattering lifetime γ. The eigenmodes of the coupled system in equation 1 are a symmetric and antisymmetric superposition of the CW and CCW-mode. The complex amplitudes of these new eigenmodes are given by equation 2:

$$\begin{aligned} a_+ &= \tfrac{1}{\sqrt{2}}\left(a_{CW}+a_{CCW}\right) = \tfrac{1}{\sqrt{2}}\frac{-\kappa s}{i\left(\Delta\omega+\frac{1}{2\gamma}\right)-\frac{1}{2\tau}} \\ a_- &= \tfrac{1}{\sqrt{2}}\left(a_{CW}-a_{CCW}\right) = \tfrac{1}{\sqrt{2}}\frac{-\kappa s}{i\left(\Delta\omega-\frac{1}{2\gamma}\right)-\frac{1}{2\tau}} \end{aligned} \tag{2}$$

From equation 2, it is clear that the eigenmodes are centered around the new eigenfrequencies $\omega = \omega_0 \pm 1/2\gamma$. They each have a linewidth of $1/\tau$, determined by the losses of the coupled microring. The results from equation 2 can be used to calculate both the CW and CCW-mode as well as the transmitted and reflected fields for the microring coupled to an input waveguide by using the relations from equation 3:

$$t = s + \kappa a_{CW} \quad \text{and} \quad r = \kappa a_{CCW} \tag{3}$$

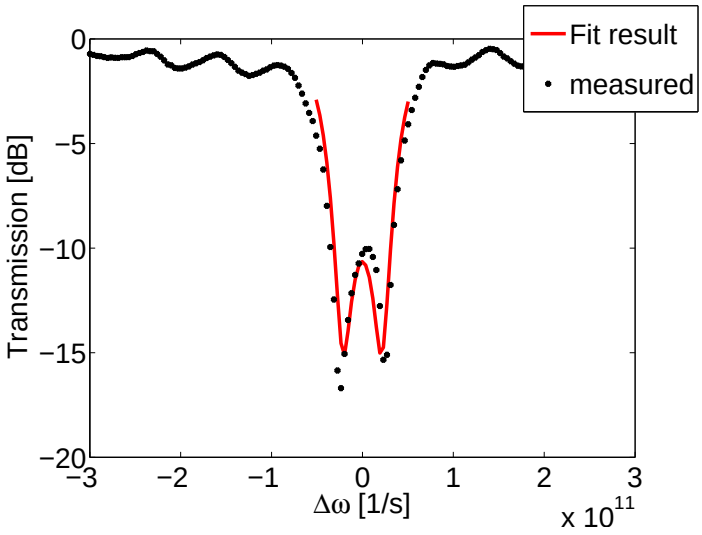

Fig. 2. Measured spectrum of all-pass microring with resonance splitting. The full line gives the theoretical transmission after fitting the model parameters

When comparing the theoretical transmission to the recorded transmission spectrum of an all-pass microring resonator, we obtain the results from figure 2. The resulting fitted parameter values indicate a quality factor of $Q = 20850$ for the eigenmodes. The mode splitting amounts to $\Delta\lambda = 79pm$ and the power coupling ratio of the directional coupler is $K^2 = 0.0332$, which corresponds well to the projected design value for critical coupling. This is summarized in table 1.

Table 1. Model parameter values

parameter		chacteristic	
κ	$2.1\times10^5 s^{-1/2}$	K^2	0.033
γ	$1.6\times10^{-11}s$	$\Delta\lambda$	$79pm$
τ	$1.7\times10^{-11}s$	Q	20850

3. Integrated interferometric circuit

As demonstrated in [11], in the context of a fiber-based system, an interferometric approach can be used to retrieve the unsplit modes of the microring resonator in an output signal. However, such a fiber-based setup is difficult to stabilize and to integrate. Therefore, we have implemented this in an integrated circuit on a single SOI-chip. A layout of the circuit is provided in figure 3. Vertical grating couplers are used to couple light from a tunable laser lightsource into the circuit and collect the power at the output. The input light excites the CW-mode in the microring resonator, which in turn excites the CCW-mode as a consequence of mode coupling. The normal modes of the microring resonator are the symmetric and antisymmetric superposition of the CW and CCW-mode, given by equation 2. If the coupling per unit time between the bus waveguide and the microring is represented by κ, the fields transmitted and reflected by the resonator are again given by equation 3. Here, $s = a_{in}/\sqrt{2}$ and $|a_{in}|^2$ is the total input power.

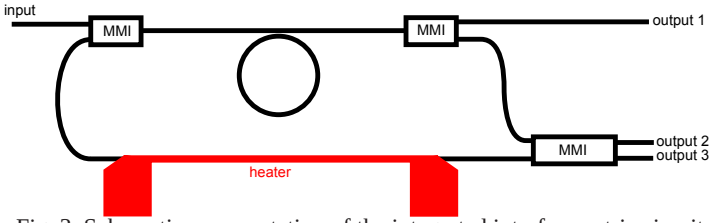

Fig. 3. Schematic representation of the integrated interferometric circuit

The input light is first passed through a 3dB combiner before coupling into the microring. The CW propagating light will couple back to the waveguide to constitute the transmitted field. The CCW propagating light will form the reflected field when coupling back to the waveguide. The input combiner acts as a splitter for the reflected light which is guided through a feedback arm towards a 2x2 multi mode interference (MMI) coupler. The transmitted light is passed to a 3dB MMI-splitter. It is split equally between output 1 and the 2x2 MMI coupler, where it is recombined with the reflected light. The signals from the 2x2 coupler are the result of interference between the transmitted and reflected fields and are collected in output 2 and 3. For the case of a perfect 2x2 MMI coupler, the fields at the output ports for given input fields E_1 and E_2 are $1/\sqrt{2}\,(E_1 \pm iE_2)$. There is a quadrature phase relationship between both output signals. We can summarize the output fields of the interferometric circuit in equation 4:

$$\begin{aligned} out_1 &= \tfrac{1}{\sqrt{2}} t \\ out_2 &= \tfrac{1}{2}\left(\tfrac{1}{\sqrt{2}} a_{in} + \kappa a_{CW} + e^{i\phi}\,\kappa a_{CCW}\right) \\ out_3 &= \tfrac{1}{2}\left(\tfrac{1}{\sqrt{2}} a_{in} + \kappa a_{CW} - e^{i\phi}\,\kappa a_{CCW}\right) \end{aligned} \tag{4}$$

Here, ϕ is the phase difference between the interfering transmitted and reflected fields. We find that output 1 is always proportional to the pass-signal of the microring resonator in the all-pass configuration. To obtain the required output signals in output 2 and 3, the phase difference ϕ between the transmitted and reflected wave has to be controlled carefully. In this case, this is done by processing a titanium-gold heater on the feedback waveguide. By setting the current through the heater, we can tune the phase difference to the required value. If it is a multiple of π, we see from equation 4 that the signals in output 2 and 3 are given by the sum of a constant and a signal proportional to the complex amplitudes of the normal modes of the resonator, given by equation 2. In other words, the spectral shape of the signals in output 2 and 3 will be identical to this of the complex amplitudes of the eigenmodes. This means we will have access to the unsplit, high-Q normal modes of the cavity. Since the detection limit of a biosensor is limited by the quality factor of the resonance [12] - higher resonator Q-factors give rise to lower detection limits - this provides a tool to improve the detection limit significantly. Even

worse, fitting errors introduced by resonance splitting can cause jumps between both modes of a split resonance that lead to false positive or even false negative results when the sensor is implemented in a lab-on-a-chip setting.

4. Fabrication and calibration

The circuit from figure 3 is designed and processed in a CMOS pilot line at imec. Using the vertical in- and output couplers on the waveguides [13], the chip can easily be measured in a fiber-to-fiber configuration. The process of depositing tuning heaters on the feedback waveguide is straightforward and requires no high-accuracy allignment steps. To limit optical losses induced by the heater metal, a polymer layer of approximately $1\mu m$ is deposited on the chip surface prior to heater definition. For this layer, the photopatternable resin Cyclotene 4022-25 [14] is used to allow the definition of windows over critical device structures. The polymer is derived from B-staged bisbenzocyclobutene (BCB) and is widely used for various post-processing steps on SOI-chips for near-infrared applications [15]. After developement, photo-BCB covering the microring, grating couplers and 2x2 MMI is removed.

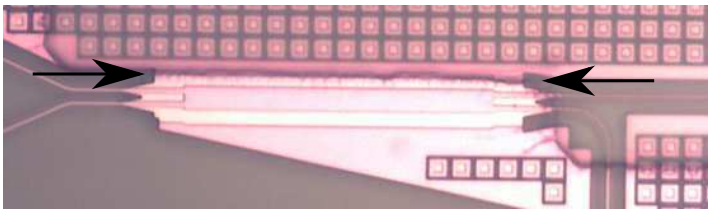

Fig. 4. Microscope image of lithographically opened BCB layer. The arrows indicate the edge of the 2x2 MMI that is covered by BCB residue

Figure 4 shows the 2x2 MMI and the edge of the BCB layer. The tuning heater is then processed on the chip with locally opened BCB cover. For that purpose, a lithographic lift-off procedure is used [16]. The heater measures 450 by $2.5\mu m$ with large contact pads for easy probing. For characterization of the tuning heater, a Mach-Zehnder-Interferometer (MZI) is used. By comparing the output intensity of the MZI to the theoretical cosine squared interference pattern for different heater currents, we were able to determine the quadratic relationship between heater current and phase change as $\phi = 0.4 rad/mA^2 \times I^2$. This confirms the phase change in the heated waveguide is proportional to the dissipated power in the metalic heater. The resulting calibration curve is shown in figure 5. A phase range of 2π is obtained for heater currents from 0 to $4mA$.

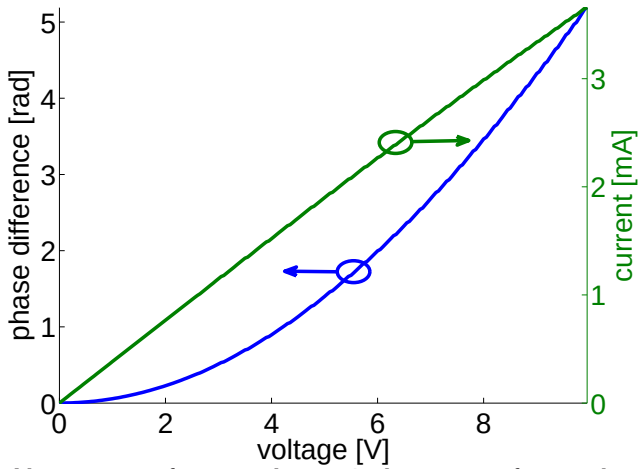

Fig. 5. Calibration curve for tuning heater. A phase range of 2π is obtained for heater currents from 0 to $4mA$

5. Experimental results

The fabricated chip with integrated interferometric circuit is mounted on a vertical optical setup for fiber-to-fiber characterization. To obtain the measured spectra, a TUNICS tunable laser source is used to generate the input signals. Output intensities are measured by a HP-8153 optical power meter. The laser wavelength is swept in 5*pm* steps while power is recorded. Setting the heater current gives us the ability to change the resonance state in the output signals from one normal mode, over the severely split intermediate state to the other normal mode.

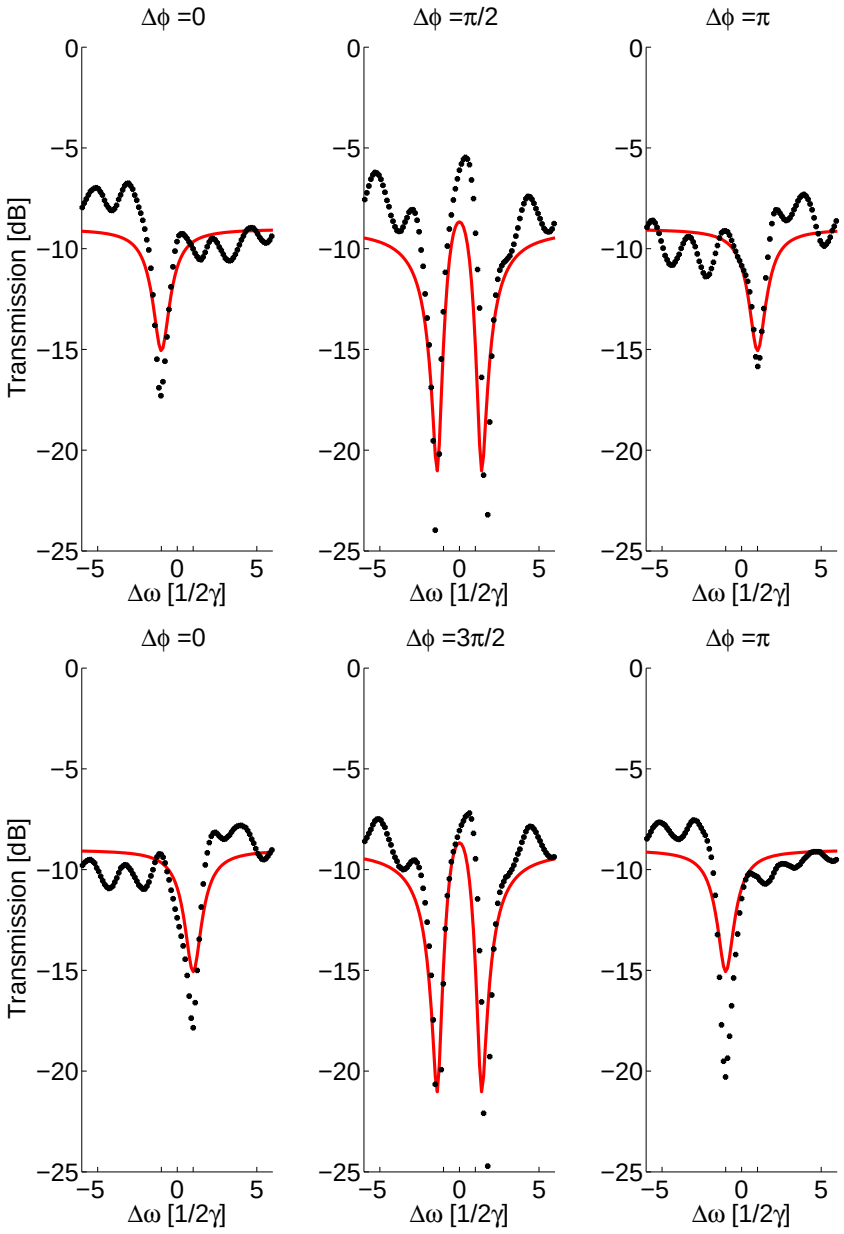

Fig. 6. Interferometric output signals for different phase difference between reflected and transmitted field: (top) output 2 (bottom) output 3. The full line gives the theoretically predicted signals and the dotted line gives the experimentally recorded power

This is demonstrated in figure 6 where recorded spectra of the output couplers are shown for different phase differences between the interfering waves. In this figure, the theoretically predicted output signals according to equation 4 are also provided. The values for the model parameters are given by table 1. The correspondence between theory and experiment shows we have a good understanding of the physical effects in the microring resonator. We have to remark the 2x2 MMI is particularly sensitive to processing variations that effect its transmission characteristics. The proximity of the BCB layer to one edge of the MMI, which is seen on figure 4, generates an assymetric coupler transmission. This results in a extra phase shift of approximately $\pi/2$ in the transmission from input port 2 to output port 3, which was determined by fitting. This phase change has already been accounted for in the theoretical model and heater currents have been adapted accordingly.

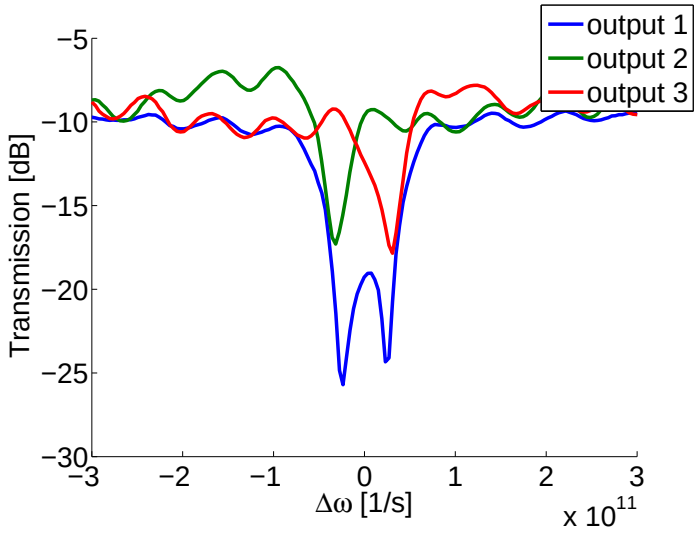

Fig. 7. Split all-pass transmission and interferometric output signals showing unsplit modes for a phase difference $\Delta\phi = 0$. Output power of output 1 has been scaled for clarity

The width and corresponding quality factors of the recorded eigenmode spectra compare favourably to those of the resonance signal in output 1, as can be seen from figure 7. When determined based on the fitted model of equation 2, we obtain a width of $50pm$ for the unsplit eigenmodes and one of $130pm$ for the split all-pass transmission. Since the limit of detection (LOD) scales with the square root of the resonance width, this technique provides a potential LOD improvement with a factor 1.6. One could argue that the total width of the transmission resonance is not a good measure for estimating detection limits. However, when the resonance splitting $\Delta\lambda$ is less than or equal to the width of the individual normal modes, splitting will be obscured while still causing significant broadening of the resonance dip. In that case, a fit to the more narrow unsplit mode revealed by this interferometric approach will always be more accurate and provide limit of detection improvements up to a factor $\sqrt{2}$, while at the same time eliminating the chance of false positive or negative detections due to intrinsic microring effects.

6. Conclusion

In this paper, we demonstrate the successful integration of an interferometric circuit to resolve resonance splitting on a SOI-chip. We also show that a simple theoretical model of coupled harmonic oscillators can adequately describe the microring mode splitting. Using a tuning heater, we can sweep the phase difference between the combining reflected and transmitted fields of the

microring and change the output signals from a severely split spectrum to the unsplit microring modes with high quality factors. The theoretical predictions are confirmed by the experiment. When comparing the output signals of the interferometric circuit to the split resonance of the all-pass microring, the resonance width is reduced by approximately a factor 3. This can result in a limit of detection improvement by a factor 1.6, while at the same time eliminating the chance of false positive or negative detections due to intrinsic microring splitting.

Acknowledgments

Sam Werquin would like to acknowledge the Special Research Fund of Ghent University (BOF-UGent) for providing a research grand. The research is also supported by the Interuniversity Attraction Poles program of the Belgian Science Policy Office 'Photonics@be'. Finally, the authors would also like to thank Thomas Van Vaerenbergh for many fruitful discussions.